Contract No. N00014-67-A-0438-0009
Project No. NR 061-135

Contract No. DAHC04-69-C-0077
ARPA Order No. 1442, Amendment 2
Program Code No. 9E30

ENTROPY LAYERS

by

Gino Moretti and Maurizio Pandolfi

POLYTECHNIC INSTITUTE OF BROOKLYN

DEPARTMENT
of
AEROSPACE ENGINEERING
and
APPLIED MECHANICS

NOVEMBER 1971

PIBAL REPORT NO. 71-33

Unclassified

Security Classification

DOCUMENT CONTROL DATA - R & D

(Security classification of title, body of abstract and indexing annotation must be entered when the overall report is classified)

1. ORIGINATING ACTIVITY *(Corporate author)*
Polytechnic Institute of Brooklyn
Dept. of Aerospace Engrg. & Appl. Mechanics
Route 110, Farmingdale, New York 11735

2a. REPORT SECURITY CLASSIFICATION
Unclassified

2b. GROUP

3. REPORT TITLE
ENTROPY LAYERS

4. DESCRIPTIVE NOTES *(Type of report and inclusive dates)*
Research Report

5. AUTHOR(S) *(First name, middle initial, last name)*
Gino Moretti
Maurizio Pandolfi

6. REPORT DATE	7a. TOTAL NO. OF PAGES	7b. NO. OF REFS
November 1971	24	10

8a. CONTRACT OR GRANT NO.
N00014-67-A-0438-0009
DAHC04-69-C-0077

b. PROJECT NO
NR 061-135

c
ARPA Order No. 1442, Amendment 2

d Program Code 9E30

9a. ORIGINATOR'S REPORT NUMBER(S)
PIBAL Report No. 71-33

9b. OTHER REPORT NO(S) *(Any other numbers that may be assigned this report)*

10. DISTRIBUTION STATEMENT
This document has been approved for public release and sale; its distribution is unlimited.

11. SUPPLEMENTARY NOTES

12. SPONSORING MILITARY ACTIVITY
Office of Naval Research
Arlington, Virginia
U.S. Army Research Office-Durham, N.C.

13. ABSTRACT

The entropy layer on a blunt-nosed cone is analyzed, in view of the difficulties it produces in numerical computations. A rule is given to determine at what distance from the nose the entropy layer is a given fraction of the shock layer, for a given free stream Mach number.

A simple and very efficient way of computing flows with strong entropy layer effects is given. It consists of inserting two streamlines representing loci of rapid changes in entropy derivatives, and forbidding differentiation across such lines.

DD FORM 1 NOV 68 1473

Unclassified

Security Classification

14 KEY WORDS	LINK A		LINK B		LINK C	
	ROLE	WT	ROLE	WT	ROLE	WT
Entropy layers Compressible flow Blunted cones Numerical analysis						

ENTROPY LAYERS

by

Gino Moretti and Maurizio Pandolfi

This research was conducted in part under the sponsorship of the Office of Naval Research under Contract No. N00014-67-A-0438-0009, Project No. NR 061-135, and in part by the Advanced Research Projects Agency, monitored by the U.S. Army Research Office-Durham under Contract No. DAHC04-69-C-0077.

POLYTECHNIC INSTITUTE OF BROOKLYN

Department

of

Aerospace Engineering and Applied Mechanics

November 1971

PIBAL Report No. 71-33

BLANK PAGE

ENTROPY LAYERS[†]

by

Gino Moretti[‡] and Maurizio Pandolfi[*]

Polytechnic Institute of Brooklyn
Preston R. Bassett Research Laboratory
Farmingdale, New York

ABSTRACT

The entropy layer on a blunt-nosed cone is analyzed, in view of the difficulties it produces in numerical computations. A rule is given to determine at what distance from the nose the entropy layer is a given fraction of the shock layer, for a given free stream Mach number.

A simple and very efficient way of computing flows with strong entropy layer effects is given. It consists of inserting two streamlines representing loci of rapid changes in entropy derivatives, and forbidding differentiation across such lines.

[†]This research was conducted in part under the sponsorship of the Office of Naval Research under Contract No. N00014-67-A-0438-0009, Project No. NR 061-135, and in part by the Advanced Research Projects Agency, monitored by the U.S. Army Research Office-Durham under Contract No. DAHC04-69-C-0077.

[‡]Professor, Dept. of Aerospace Engineering and Applied Mechanics.

[*]Postdoctoral Fellow, Dept. of Aerospace Engineering and Applied Mechanics; on leave of absence from the Politecnico di Torino, Italy.

TABLE OF CONTENTS

LIST OF ILLUSTRATIONS

I. INTRODUCTION

Strong entropy gradients tend to appear near the surface of a vehicle flying at a supersonic speed. The vorticity in the affected region is very high. Vortical layers are produced by either one of two different and independent effects, or by a combination of both:

a) If the vehicle has a pointed nose and flies at an angle of attack, the streamlines proceeding from the shock wave run very close to their original meridional plane until, at a small distance from the body, they turn towards the leeward symmetry plane, piling up in increasing number on a layer of decreasing thickness. A cross-section of the flow shows the projections of the stream-lines converging to a point on the leeward plane, called Ferri's vortical singularity. Each streamline carries a constant value of entropy. By and large, the entropy behind the shock wave diminishes from the windward to the leeward symmetry plane. Therefore, in a thin layer on the leeward side of the body, the entropy decreases in a radial direction from the body surface outwards. In an inviscid flow, such a vortical layer becomes vanishingly thin at the vortical singularity.

b) If the vehicle has a blunted nose and flies at no incidence, the bow shock starts as a normal shock on the symmetry line and bends towards the free stream characteristic cone. By and large the entropy behind the bow shock decreases with increasing distance of the shock point from the body axis. Streamlines from the frontal portion of the bow shock remain confined within a small distance from the body through all its length since more and more mass flow is swallowed through the receding shock wave. Such streamlines define a layer across which the entropy varies from its normal shock value to practically its free stream value, and which is strongly vortical. Its thickness, relative to the shock layer thickness, decreases with increasing distance from the nose.

almost conical pattern. With increasing distances from the nose, the shock tends to become the conical shock related to a pointed cone with its apex at Q (the intersection of the symmetry axis with the conical section of the body). The entropy behind the shock reaches a minimum at a point L, which can be located approximately at the intersection of the tangent to the shock at F with the conical shock, QG. The mass flow through the shock between A and L is squeezed between the body, DB and the streamline, LE issuing from L. At any section, BG of the shock layer, the total mass flow equals the mass flow through the entire shock, AG. For the present evaluation, we assume that the vertical layer is defined by BE (whose thickness, in terms of nose radii, is δ) and that the flow across EG is conical. Let b and d be the cone thickness, GE and the shock layer thickness, BG, respectively at the same station. Given a value of δ/d, we want to evaluate at what station, H, such a value occurs.

In the flow about a pointed cone, the distributions of density (ρ) and axial velocity (w) at a given station are qualitatively shown in Fig. 2 (solid lines). We assume that in the entropy layer (BE) density

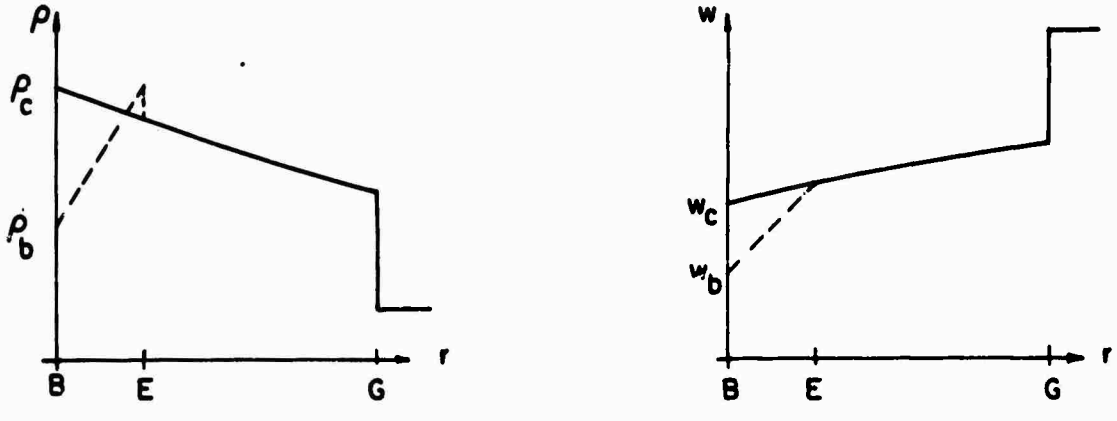

Fig. 2 Approximate Distributions of Density and Axial Velocity Across Shock Layers.

Hayes and Probstein[1] call it the "entropy wake". A more popular name is "entropy layer".

Here we intend to discuss the problem posed by an entropy layer in a numerical analysis.

II. ESTIMATE OF THE THICKNESS OF THE ENTROPY WAKE

A crude, but significant, estimate of the thickness of the entropy layer relative to the shock layer thickness when the first is at least one order of magnitude smaller than the latter can be obtained as follows: Consider Fig. 1, which shows a section of a sphere-cone vehicle, ND being the spherical and DB the conical portion. The sphere controls the shape of the bow shock between A and F, the latter being the shock point on the characteristic issuing from D. After F, the shock wave evolves into an

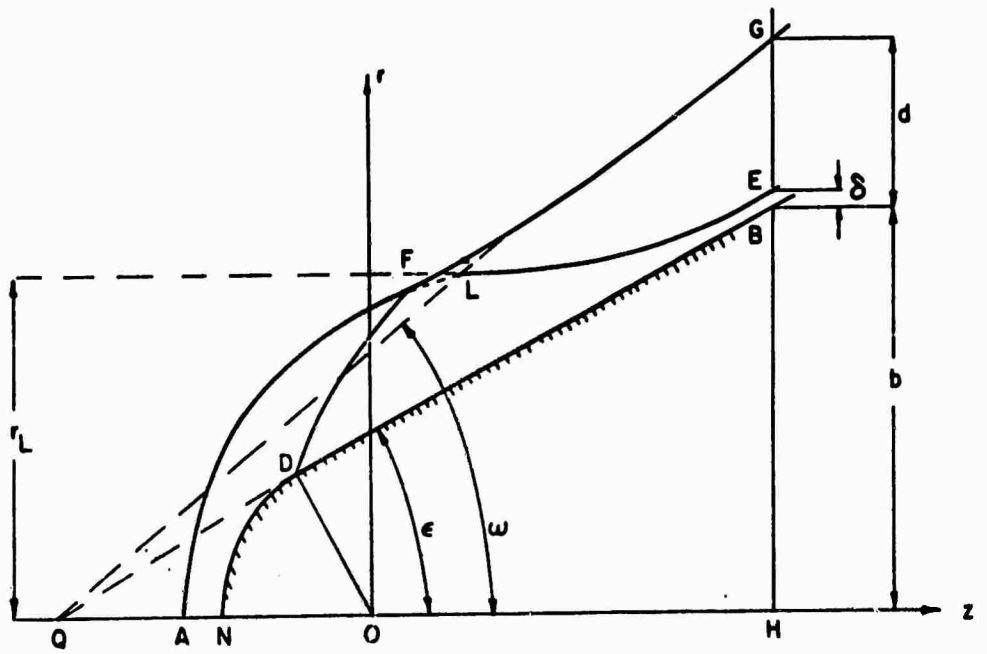

Fig. 1 Blunt-Nosed Cone Shock Layer.

almost conical pattern. With increasing distances from the nose, the shock tends to become the conical shock related to a pointed cone with its apex at Q (the intersection of the symmetry axis with the conical section of the body). The entropy behind the shock reaches a minimum at a point L, which can be located approximately at the intersection of the tangent to the shock at F with the conical shock, QG. The mass flow through the shock between A and L is squeezed between the body, DB and the streamline, LE issuing from L. At any section, BG of the shock layer, the total mass flow equals the mass flow through the entire shock, AG. For the present evaluation, we assume that the vortical layer is defined by BE (whose thickness, in terms of nose radii, is δ) and that the flow across EG is conical. Let b and d be the cone thickness, GE and the shock layer thickness, BG, respectively at the same station. Given a value of δ/d, we want to evaluate at what station, H, such a value occurs.

In the flow about a pointed cone, the distributions of density (ρ) and axial velocity (w) at a given station are qualitatively shown in Fig. 2 (solid lines). We assume that in the entropy layer (BE) density

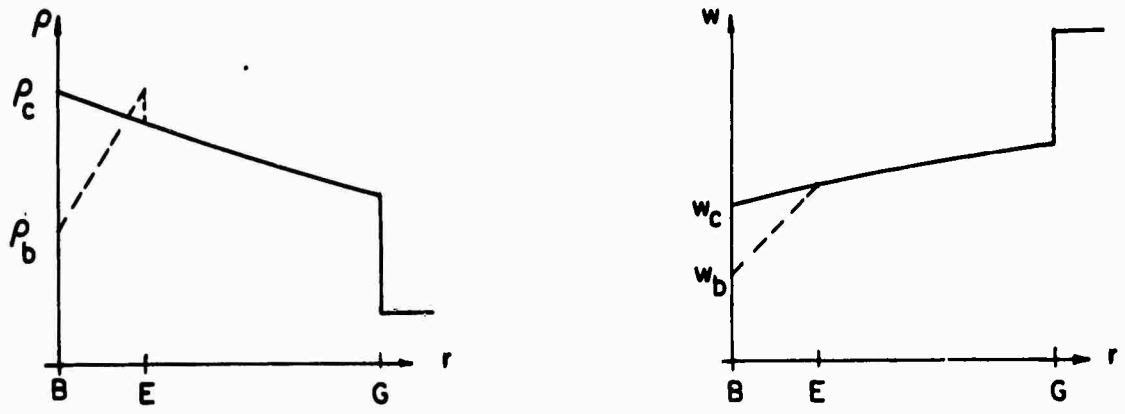

Fig. 2 Approximate Distributions of Density and Axial Velocity Across Shock Layers.

and axial velocity have the qualitative behavior shown in Fig. 2 by dotted lines. In particular, we assume that ρ and w can be approximated by linear functions

$$\rho = \rho_B + (\rho_c - \rho_B)y \quad , \quad w = w_B + (w_c - w_B)y \tag{1}$$

where

$$y = \frac{r - b}{\epsilon} \tag{2}$$

ρ_c and w_c are the pointed cone values and ρ_B, w_B are the actual values of density and axial velocity at the body surface, respectively. The values of ρ_B and w_B can be evaluated as follows: We assume that the flow about the pointed cone with the same cone semi-angle ε, and the same free stream Mach number, M_∞, as in the blunted case, is known. In particular, we know the shock angle, σ, and the values of pressure, density and velocity at the cone surface (denoted by a subscript, c, in what follows). The stagnation pressure at B is the same as at A behind the shock,

$$p_{o_B} = \left(\frac{\gamma + 1}{2} M_\infty^2\right)^{\frac{\gamma}{\gamma-1}} \left[\frac{\gamma+1}{2\gamma M_\infty^2 - (\gamma-1)}\right]^{\frac{1}{\gamma-1}} p_\infty \tag{3}$$

The static pressure, p_B at B is assumed to be equal to the conical flow pressure at B, p_c. The local Mach number, M_B at B follows:

$$M_B^2 = \frac{2}{\gamma-1}\left[\left(\frac{p_{o_B}}{p_B}\right)^{\frac{\gamma-1}{\gamma}} - 1\right] \tag{4}$$

The local speed of sound, a_B at B is given by

$$a_B = a_o \left(1 + \frac{\gamma-1}{2} M_B^2\right)^{-\frac{1}{2}} \tag{5}$$

where a_o is the stagnation speed of sound in the free stream. Consequently,

$$\rho_B = \gamma p_B / R a_B^2 \tag{6}$$

and

$$w_B = M_B a_B \cos\theta \tag{7}$$

The mass flow, m_s between B and E is thus obtainable from

$$m_s = 2\pi \int_0^1 \rho w(b + \delta y)dy \tag{8}$$

with ρ and w defined by (1). Note that, at this stage, neither b nor δ have been determined yet.

Now, m_s can be computed as

$$m_s = \pi \rho_\infty a_\infty M_\infty r_L^2 \tag{9}$$

From (8) and (9)

$$(\frac{r_L}{d})^2 = \frac{2}{\rho_\infty a_\infty M_\infty} \frac{\delta}{d} \int_0^1 \rho w(\frac{b}{d} + \frac{\epsilon}{d} y)dy \tag{10}$$

follows. Since

$$\frac{b}{d} = \frac{\tan\epsilon}{\tan\theta} \tag{11}$$

we know r_L/d as a function of δ/d. To get d, once δ/d has been prescribed, r_L must be determined. At this stage, we make use of an existing blunt body computational program[2] coupled with a computation of the supersonic flow by the method of characteristics to determine r_L for a sphere as a function of M_∞ and the location of point D (that is, as a function of ϵ). Finally, b is obtained from (11) and the value of z (measured from the center of the nose in terms of nose radii) is

$$z = \frac{d + b}{\tan\theta} - \frac{1}{\sin\epsilon} \tag{12}$$

as a function of M_∞ and θ.

Results of the computation are shown in Figs. 3 and 4 for $\delta/d = 0.1$ and $\delta/d = 0.05$, respectively. The results are almost independent of the free stream Mach number.

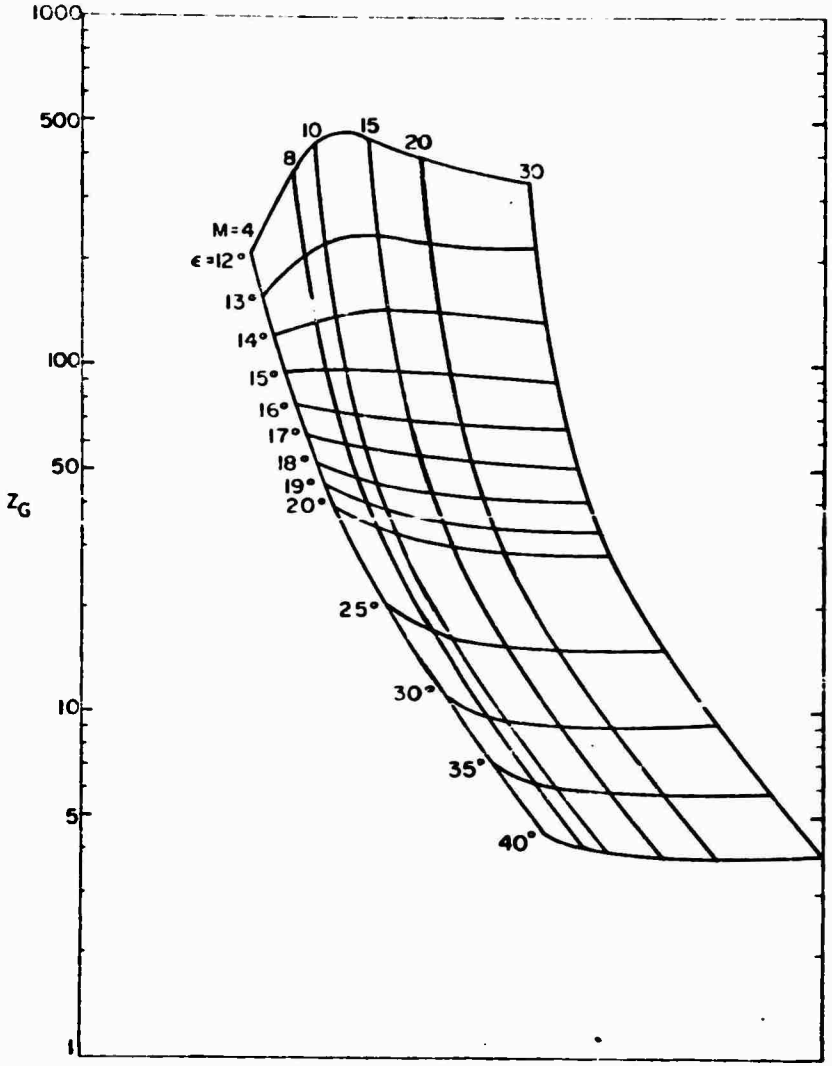

Fig. 3. Distance from Nose at Which Entropy Layer Thickness is 1/10 of Shock Layer Thickness

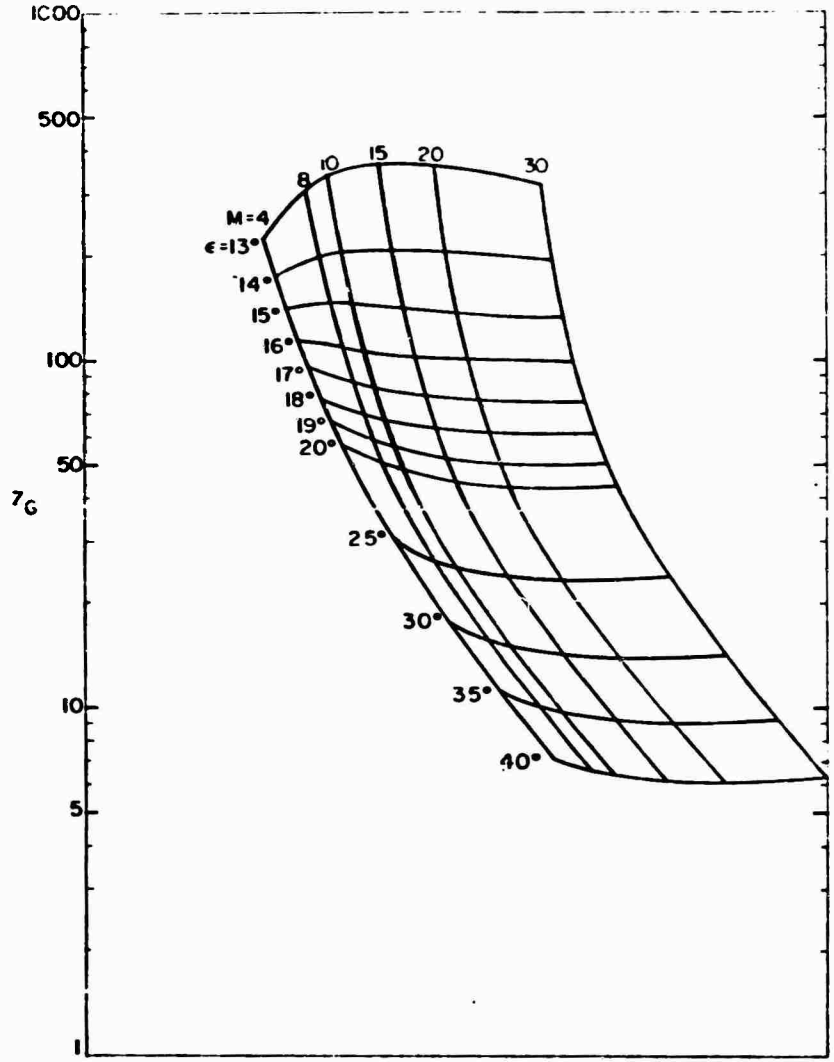

Fig. 4. Distance from Nose at Which Entropy Layer Thickness is 1/20 of Shock Layer Thickness

It is clear from the figures that, if the cone angle is not very small, vorticity tends to concentrate in a narrow layer at relatively short distances (10, 20 nose radii) from the nose. Catastrophic effects may result in a numerical computation*, unless proper steps are taken.

III. PRELIMINARIES FOR THE NUMERICAL ANALYSIS

We now draft a numerical analysis of the steady, axisymmetric, inviscid, supersonic flow about a sphere-cone configuration, obviously not to repeat a computational exercise which has been performed an endless number of times in the last decade, but with a specific goal in mind. The analysis should be for us a guideline to generate a computer program for three-dimensional flows, apt to work economically and safely for very long bodies, particularly when the entropy layer becomes very thin. The results of Section II show that such is the case when the body slope is high, even at relatively short distances from the body nose.

The method of characteristics is ruled out because it is unsuitable for three-dimensional problems. We choose a technique which, in principle, is patterned on the same general methods we used in a great variety of problems. The computation proceeds stepwise from a cross-section, normal to the z-axis of symmetry, to another normal cross-section, their distance, Δz, being defined to comply with the Courant-Friedrichs-Lewy rule[3]. A fixed number of nodal points is considered, at all cross-sections, between body and shock. The first point lies on the body, the last on the shock; all other points (interior points) are in the shock

*Let us keep in mind that in a typical hypersonic transport configuration, the fuselage runs for 125 nose radii before the wing-body junction. In what follows, we will see that the computation may actually degenerate at about 20 nose radii. The most affected quantity is the Mach number which can become less than 1 in spots, bringing the computation to a halt.

layer. The nodes are not necessarily equally spaced in the physical (r,z) plane. However, a transformation of coordinates is used to generate a computational (X,Z) plane in which the distance between shock and body is normalized and the nodes are equally spaced in the X-direction. The Z coordinate is simply taken equal to z.

In principle[4], three different integration schemes should be used for interior points, body points, and shock points, respectively. The equations of motion to be integrated at interior points are

$$\begin{cases} uP_r + wP_z + \gamma(u_r + w_z + \frac{u}{r}) = 0 \\ uu_r + wu_z + \tilde{J}P_r = 0 \\ uw_r + ww_z + \tilde{J}P_z = 0 \\ uS_r + wS_z = 0 \end{cases} \tag{13}$$

where

u,w are the velocity components in the r,z directions, respectively

P is the logarithm of the pressure

$\tilde{J}$ is the ratio between pressure and density, and S is the entropy*.

With the transformation

$$\begin{aligned} X &= X(r,z) \\ Z &= z \end{aligned} \tag{14}$$

the following equation in matrix form is obtained:

$$f_Z = Af_X + B \tag{15}$$

*All quantities are made non-dimensional. Pressure and densities are scaled to their values, p_∞ and ρ_∞, in the free stream. Velocities are scaled to $(p_\infty/\rho_\infty)^{\frac{1}{2}}$. Lengths are scaled to the nose radius. The non-dimensional entropy is the difference of P and γ times the logarithm of density. Temperatures are also expressed in terms of the free stream temperature, so that $\tilde{J}$ is the non-dimensional temperature. The speed of sound, a, equals $\sqrt{\tilde{J}}$ in the free stream and $\sqrt{\gamma\tilde{J}}$ at any other point.

$$f = \begin{bmatrix} P \\ w \\ u \\ S \end{bmatrix} \quad , \quad A = \begin{bmatrix} -E & \gamma BX_r & -CX_r & 0 \\ DX_r & -E & GX_r & 0 \\ -\mathcal{J}X_r/w & 0 & -F & 0 \\ 0 & 0 & 0 & -F \end{bmatrix} \quad , \quad B = \begin{bmatrix} -\gamma Bw/r \\ \gamma D/r \\ 0 \\ 0 \end{bmatrix} \tag{16}$$

with

$$\mathcal{J} = 1/(w^2-a^2), \quad B = \mathcal{J}u, \quad C = \gamma\mathcal{L}w, \quad D = B\mathcal{J}$$
$$E = X_z + BwX_r, \quad F = X_z + \mathcal{J}X_r, \quad G = \mathcal{J}a^2 \tag{17}$$

A two-level, predictor-corrector integration scheme suggested by MacCormack and discussed in Ref. 4 is applied to (15).

To obtain an equation for P, at body and shock points, we observe first that the first three equations obtainable from (15) combine into two characteristic equations:

$$\pm a^2\beta P' - \gamma w^2 \tau' + \frac{\gamma a^2 \Delta}{r} u(\pm\beta w - u) = 0 \tag{18}$$

with

$$\beta = \sqrt{M^2-1} \tag{19}$$

In (18), primes mean derivatives with respect to z, evaluated along the characteristics, defined by

$$\mathcal{L} = \frac{dX}{dZ} = X_z + \mathcal{J}uwX_r \mp \mathcal{J}a^2\beta X_r \tag{20}$$

respectively. At a body point, (18) can be written in the form:

$$P_Z = -\mathcal{L}P_X + \frac{\gamma}{\beta}\left[\frac{w^2}{a^2}\mathcal{J}\tau_X - \frac{\beta}{r}u(\beta w - u)\right], \quad \mathcal{L} = X_r[\mathcal{J}(uw-a^2\beta)-\tau] \tag{21}$$

since $\tau_Z = 0$, $X_z = -\tau X_r$ on the cone surface.

Equation (21) is integrated using a two-level, predictor-corrector scheme similar to the one used for (15); however, the X-derivatives are approximated by one-sided differences at both levels. In the present problem, P is the only quantity to be determined by direct integration at a body point. Once P is obtained, $\mathcal{J}$ is immediately available from

$$\mathcal{J} = \exp\left[\frac{\gamma-1}{\gamma}P + \frac{S}{\gamma}\right] \tag{22}$$

since S is constant along the body. Then the modulus of the velocity,

q is obtained from the equation expressing the conservation of total enthalpy,

$$q^2 = \frac{2\gamma}{\gamma-1}(\tilde{J}_o - \tilde{J}) \tag{23}$$

and the two velocity components follow:

$$w = q\cos\varepsilon, \quad u = q\sin\varepsilon \tag{24}$$

At a shock point, (18) is used in conjunction with the Rankine-Hugoniot conditions:

$$P = \rho_n \frac{2\gamma M_{n\infty}^2 - (\gamma-1)}{\gamma+1}, \quad \tilde{u} = \tilde{u}_\infty \frac{(\gamma-1)M_{n\infty}^2 + 2}{(\gamma+1)M_{n\infty}^2} \tag{25}$$

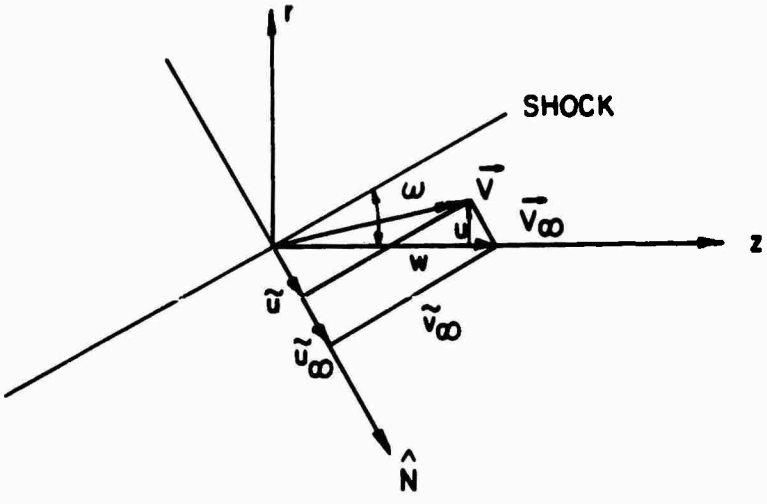

Fig. 5 Velocity Components at a Shock Point.

where

$$M_{n\infty} = M_\infty \sin\lambda = M_\infty\sigma/\nu, \quad \sigma = \tan\lambda, \quad \nu = (1+\sigma^2)^{\frac{1}{2}} \tag{26}$$

$$\tilde{u}_\infty = v_\infty\sigma/\nu \tag{27}$$

see Fig. 5. Since X=constant along the shock, the Rankine-Hugoniot conditions can be differentiated with respect to Z, yielding

$$P_Z = \frac{4\gamma M_{n\infty} M_\infty}{2\gamma M_{n\infty}^2 - (\gamma-1)} \frac{\sigma_Z}{\nu^3} \tag{28}$$

$$\tilde{u}_z = V_\infty \left[\frac{\gamma-1}{\gamma+1} - \frac{2}{(\gamma+1)M_{n\infty}^2} \right] \frac{\sigma_z}{\nu^3} \tag{29}$$

In addition,

$$\begin{cases} \tilde{u} = (w\sigma-u)/\nu \quad , \quad \tilde{v} = \tilde{v}_\infty = (w+u\sigma)/\nu \\ u = (\sigma\tilde{v}-\tilde{u})/\nu \quad , \quad w = (\sigma\tilde{u}+\tilde{v})/\nu \end{cases} \tag{30}$$

so that

$$\tilde{u}_z = (w+u\sigma)\frac{\sigma_z}{\nu^3} + (w_z\sigma-u_z)/\nu = \tilde{v}_\infty(\sigma_z/\nu^3) + (w_z\sigma-u_z)/\nu \tag{31}$$

By replacing (28), (29) and (31) into (18), the following equation for σ_z is obtained:

$$\sigma_z = \nu^3 \frac{\Delta(\sigma P_x + wu_x - uw_x) + \Delta u a^2 (u+w\beta)/r}{-2\sigma(\beta/\nu)/(\frac{\sigma^2}{\nu^3} - \frac{\gamma-1}{2V_\infty^2}) - (u^2+w^2)\nu + \tilde{v}V_\infty(\frac{\gamma-1}{\gamma+1} - \frac{2\gamma\nu^2}{(\gamma+1)\sigma^2 V_\infty^2}) + \tilde{u}V_\infty\sigma} \tag{32}$$

$$= X_r[\Delta(uw+a^2\beta) - \sigma] \tag{33}$$

Equation (32) is again integrated by a predictor-corrector scheme, whose first level yields

$$\bar{\sigma} = \sigma(Z) + \sigma_Z(Z)\Delta Z \quad , \quad \bar{c} = c(Z) + \tfrac{1}{2}[c(Z)+\bar{c}]\Delta Z \tag{34}$$

(c being the r-coordinate of the shock) and whose second level yields

$$\begin{cases} \sigma(Z+\Delta Z) = \tfrac{1}{2}[\sigma(Z) + \bar{\sigma} + \bar{\sigma}_Z \Delta Z] \\ c(Z+\Delta Z) = \tfrac{1}{2}[c(Z)+\bar{c}+\tfrac{1}{2}(\sigma_Z+\bar{\sigma}_Z)\Delta z] \end{cases} \tag{35}$$

All values used in the right-hand side of (32) to obtain $\bar{\sigma}_Z$ are values obtained at the end of the predictor step.

The computation of body points and shock points described above uses the concept of characteristics to provide the best possible equations for determining P on the body and σ_Z on the shock, without requiring iterations. Its code is easily inserted into the same predictor-corrector double loop used for interior points. Therefore, it provides the same advantages as the computation based on a direct use of characteristics,

first proposed by one of the authors[5], but it does not require special subroutines, iterations, interpolations, and it saves computational time. The idea has been suggested by Kentzer[6] for a first order accurate scheme, but, to our knowledge, so far it has not been exploited to its full capacity. This is what we intend to do by incorporating it into a predictor-corrector scheme, as outlined above, in order to achieve higher accuracy and maintain a logical consistency with the interior point computation. See also Refs. 7 and 8 for further details and comparisons with other methods.

A careful treatment of the boundary conditions (that is,a choice of equations which emphasize the role played by the vanishing of the normal velocity component on a rigid wall, by the Rankine-Hugoniot conditions at the shock and the propagation of signals along the characteristics, together with the elimination of all equations which contain some element not directly relatable to the boundary conditions) is a major factor of success[9]. One may be tempted to substitute the body point treatment described above by an integration scheme, similar to the one used at interior points, where at both (predictor and corrector) levels the x-derivatives are approximated by one-sided differences from the interior of the flow field. Accordingly, one could try to introduce the conditions of vanishing normal velocity component by combining the two equations for u and w in order to provide a single equation for the tangential component; this is easy to do because of the simple geometry of the cone. We can avoid him the trouble. We have repeated all the runs described below using the latter scheme and we have found a definitive worsening of the computed values in all cases. Pressure is a particularly sensitive parameter and the use of (21) is imperative, particulary when one is concerned with reducing the number of computational nodes to a minimum.

Initial conditions will be specified along a straight line, normal

to the z-axis, issuing from the contact point between the sphere and cone.

All examples given in the following discussion have been computed for a 25° sphere-cone at a free stream Mach number equal to 10.6.

IV. FIRST COMPUTATION WITH EQUALLY SPACED NODES

We begin by applying the numerical technique outlined in Section III to a mesh with a constant number of nodes, equally spaced between shock and body. Equation (14) is thus specified as

$$\begin{cases} X = \dfrac{r-b}{c-b} \\ Z = z \end{cases} \tag{36}$$

where b and c are the r-coordinates of body and shock, respectively. With n intervals between body and shock, $\Delta x = 1/n$. Runs made for n=10,20 and 30 degenerate rapidly. At a first sight, it appears that the results improve with increasing number of nodes. However, reasons of economy (particularly in view of extensions to three-dimensional problems) force n to be limited to a maximum of 20, and it would be desirable not to exceed n=10.

To get a better insight into the degenerative process, we plot some entropy distributions at constant values of z for n=10,20 and 30 (Figs. 6,7 and 8, respectively).

In all cases, the qualitative behavior of the entropy distributions is good at small values of z. The entropy minimum moves towards the body. However, the minimum value itself decreases,in contrast with the constancy of entropy along streamlines. Further on, an accumulation of truncation errors, due to an evident lack of resolution, produces oscillations in the entropy distribution, which obviously have no physical

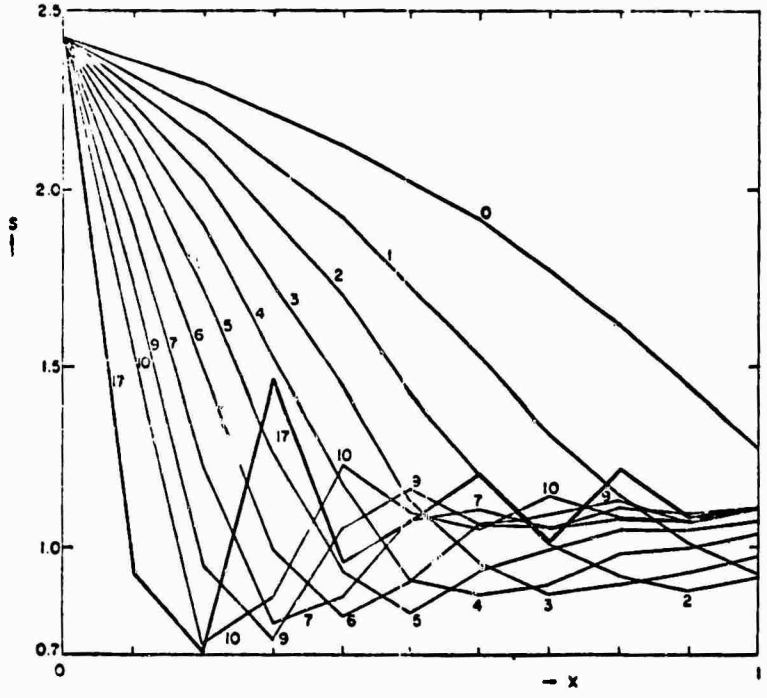

Fig. 6. Entropy Distribution Across Shock Layer at Different Distances from the Nose; n=10

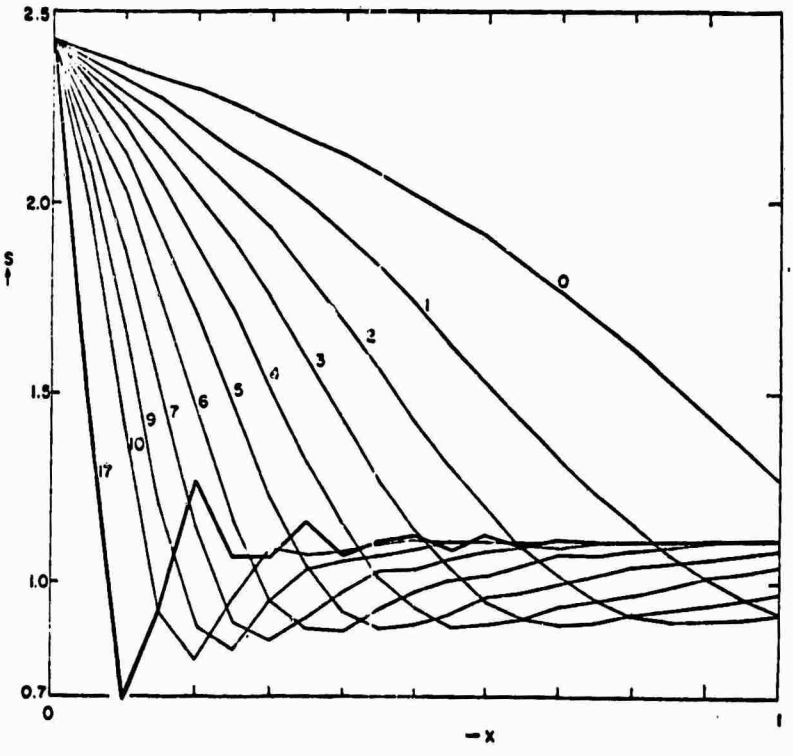

Fig. 7. Entropy Distribution Across Shock Layer at Different Distances from the Nose; n=20

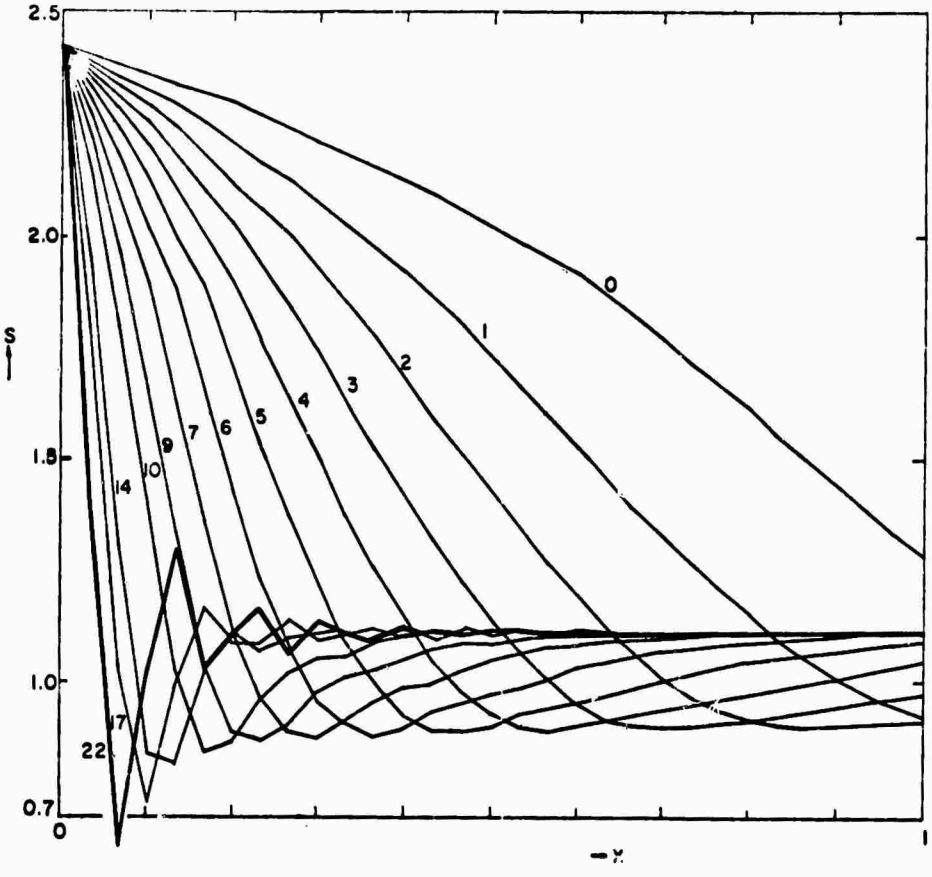

Fig. 8 Entropy Distribution Across Shock Layer at Different Distances From the Nose; n = 30.

meaning. The pressure (well controlled by the shock and body boundary conditions) and, consequently, the streamline slope are little affected. The Mach number, which depends on entropy through the speed of sound, becomes erratic.

The efficiency of the technique, according to the above mentioned standards, is to be considered poor, at the most.

V. SECOND COMPUTATION WITH STRETCHING OF COORDINATES

High truncation errors appear in regions where S_{XX} is very high. Obviously, if X is a linear function or r, as in (36), S_{XX} is high when

S_{rr} is high. By stretching the node distribution so that equally spaced nodes in the computational plane correspond to unevenly spaced nodes in the physical space, with accumulation of nodes in the regions of highest S_{XX}, the corresponding values of S_{XX} can be kept sufficiently small. Stretching is useful to maintain accuracy without increasing the total number of nodes to non-economical figures. However, stretching has its shortcomings. The X(r,z) function must be analytical, so that itself and its first derivatives are defined exactly at each node. Otherwise, the truncation errors which are reduced in the differentiations with respect to X grow bigger in the differentiation of X with respect to r and z. To define analytically a function X(r,z) which concentrates nodal points near the line of minimum entropy and without leaving other regions of the shock layer bare of nodes, is not an easy task. We were able to define a suitable stretching function and to choose its parameters to satisfy our needs in the sample case. However, it seems to us that the choice of parameters cannot be made a permanent, automatic, safe feature of a program intended to deal with arbitrary geometries in a wide range of Mach numbers. Therefore, we discarded the stretching concept as impractical.

VI. THIRD COMPUTATION WITH TWO COMPUTATIONAL REGIONS

The next attempt towards increased efficiency makes use of a concept, stemming from our experiences in shock calculations: wherever a function to be computed undergoes too rapid changes, better results are obtained by replacing the latter by discontinuities. Let us see how the concept can be put to work in the present problem.

Figure 9 (upper part) shows a qualitatively correct entropy distribution across the shock layer in the vicinity of the point of minimum entropy. The lower part of Fig. 9 shows the corresponding

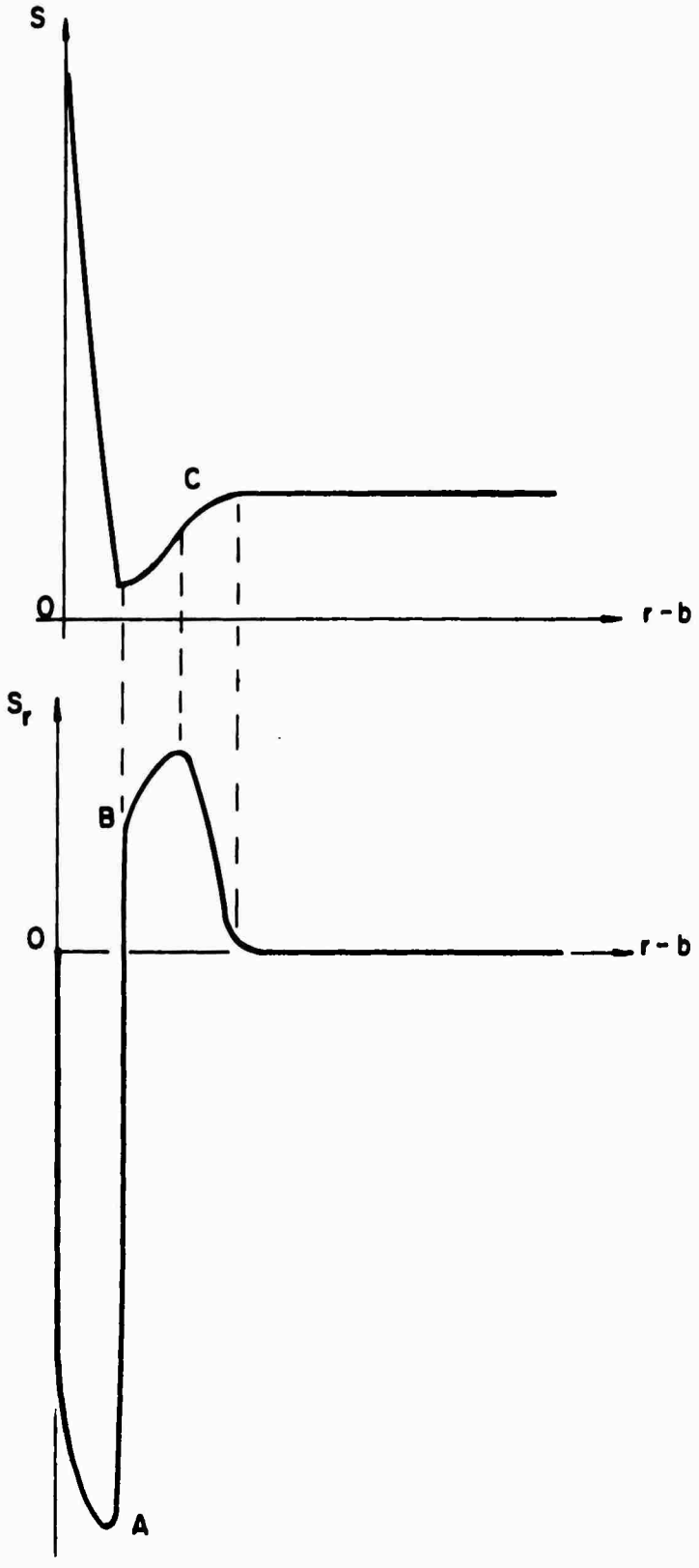

Fig. 9 Entropy and Its Radial Derivative Across a Shock Layer

qualitative behavior of S_r. The arc AB in the S_r distribution is not exactly vertical; that is, S_r is not discontinuous. However, for practical numerical calculations, it seems convenient to approximate AB by a discontinuity, so that in the physical space we may look for a line along which S_r can jump, S being continuous across it. Such a line is not a contact discontinuity, but, according to well-known principles, must be a streamline.

Consequently, we modified the program used in Section IV as follows: As the point of minimum entropy on the shock is detected, the corresponding streamline is used as a divider between two segments of the r-axis. In each segment, the r-coordinate is normalized in a way similar to (36). The nodes are equally spaced in each segment, but the spacing is different from one segment to the other. The number of nodes in each segment is determined following the same general outline described in Ref. 10. The region between the dividing line and the shock is first covered by 3 nodes. The number of nodes is automatically increased as the region grows bigger. In the region between the body and the dividing line the number of nodes is initially the same as in the original single region, and then is decreased automatically, as the region narrows. Two points are located on the dividing line, at both sides of it. The values of any physical quantity are the same on either side of the dividing line. The derivatives are approximated by one-sided finite differences computed on one side of the line at the predictor step and on the other side at the corrector step. The entropy is not calculated, but kept constant along the line, whose location is obtained by integrating the equation:

$$\frac{dr}{dz} = \frac{u}{w} \tag{37}$$

The results are very satisfactory. Not more than 20 nodes are needed to get the entropy distribution shown in Fig. 10. The entropy

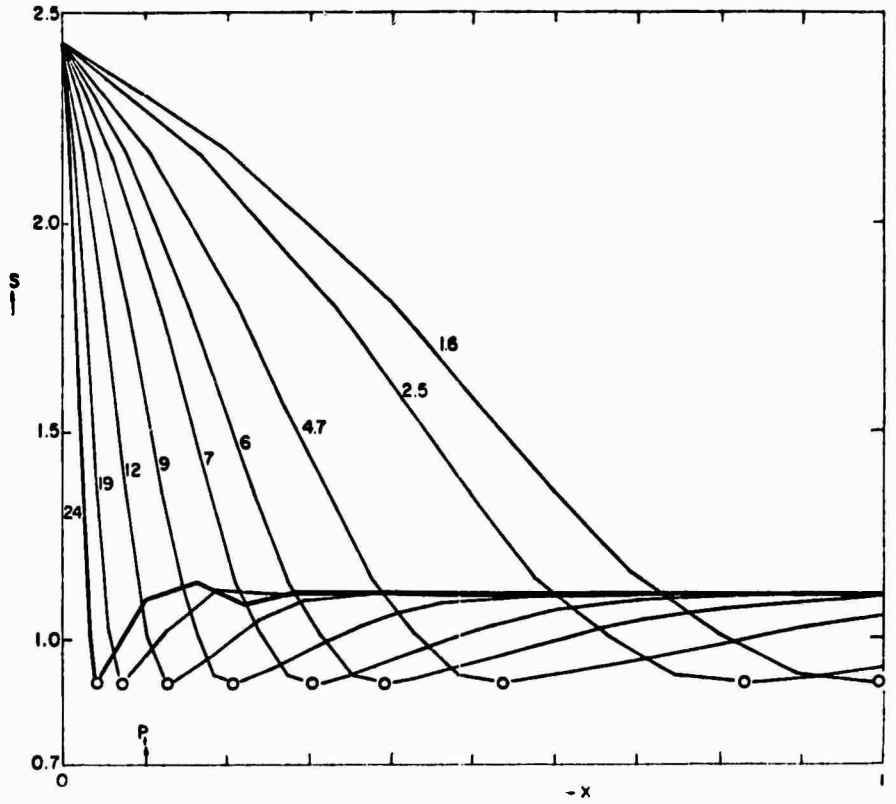

Fig. 10 Entropy Distribution Across Shock Layer at Different Distances From the Nose; Two Region Calculation.

minimum is properly carried along a streamline; no signs of deterioration appear except at a stage where the entropy layer thickness is already so small to justify neglection. The inner region is then eliminated and the body point is given the values of the first point, P_1 next to the dividing line on the outer side. Physically, this amounts to neglecting the effects of a very thin layer of hot and rarefied gas on the remaining flow. The procedure is obviously justified, because the neglected layer carries very little momentum, when compared with the rest of the shock layer. Numerically, the computation may proceed indefinitely and uneventfully.

VII. FOURTH COMPUTATION, WITH A FLOATING MINIMUM ENTROPY LINE

For axisymmetric problems, the two region approach outlined in Section VI could be the optimum one. Probably not so for three-dimensional problems. The logic and bookkeeping of the program could become too complicated.

The two region analysis, though, proved that the most sensible point in the entropy wake lies where the entropy gets its minimum value and that such a point should be treated explicitly. If we turn back to the concept of a single region with equally spaced points, as in Section IV, we can think of inserting an extra point moving along the minimum entropy line, which would thus move among the computational nodes and should be computed explicitly.

Fig. 11 shows four nodes surrounding the point of minimum entropy, A.

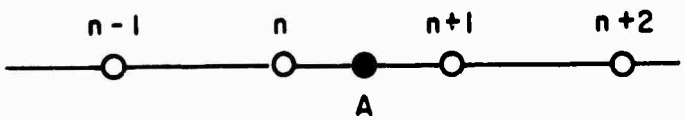

Fig. 11 Nodes Around a Point of Minimum Entropy.

At all nodes, P is computed as described in Section IV since the P-distribution is very smooth. At A, P is interpolated linearly from the neighboring points; so is the velocity slope, which is a direct consequence of the pressure distribution, and therefore smooth; S is kept constant. Temperature, speed of sound, Mach number and modulus of velocity at A follow. The flow is thus completely known at A. To compute

the right-side derivative at n or the left-side derivative at n+1 for S, u and w, the values at A and n, or at n+1 and A are used, respectively, if the distance between A and n (or n+1 and A) is larger than 1/10 of the mesh interval; otherwise, the values at n (or n+1) are interpolated from the values at A and n-1 (or n+2), at the same (predictor or corrector) level. The latter device is the simplest way to avoid erratic values of the derivatives if the denominators become too small. Occasional violations of the Courant-Friedrichs-Lewy rule[3] are harmless.

The results are shown in Figs. 12 and 13 for the cases of 10 and 20 intervals, respectively. The entropy distribution is definitively much better than in the corresponding runs described in Section IV (compare line 19 of Fig. 12 with line 17 of Fig. 6 and line 19 of Fig. 13 with line 17 of Fig. 7). It seems that the device is sufficient to maintain the errors in entropy within safe limits, without lengthening the computation and complicating the logic.

VIII. FINAL COMPUTATION - CONCLUSIONS

The improvement brought in by the explicit tracking of the line of minimum entropy at practically zero cost suggested a further improvement of the same nature, in order to eliminate the remaining wiggles of Figs. 12 and 13. Such wiggles are evidently due to the fact that the curvature of the entropy distribution is also high around point C (Fig. 9). A second streamline is tracked from the shock, starting at the first point where S approaches its asymptotic value (to within a given tolerance). The treatment of the second special point is the same as described in Section VII for point A. The results are shown in Fig. 14 for the case

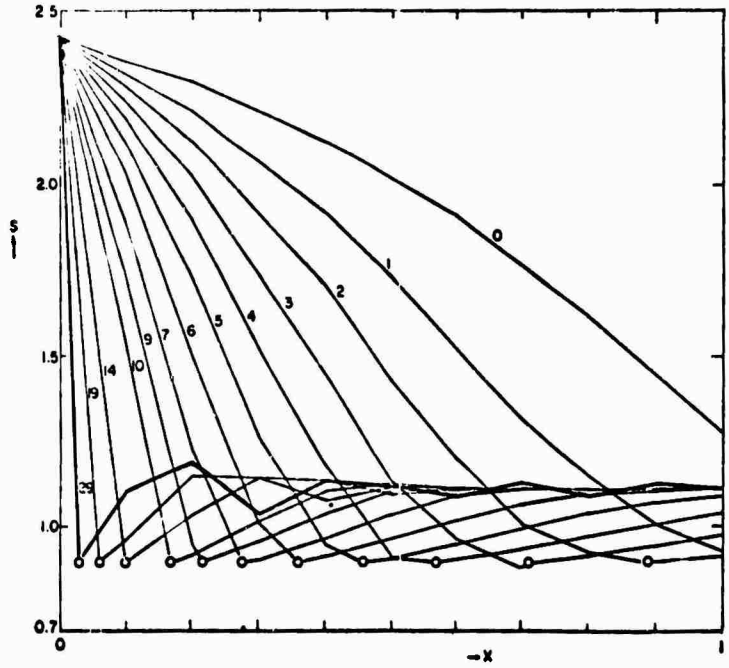

Fig. 12. Entropy Distribution Across Shock Layer at Different Distances from the Nose; Explicit Fit of the Point of Minimum Entropy; n=10

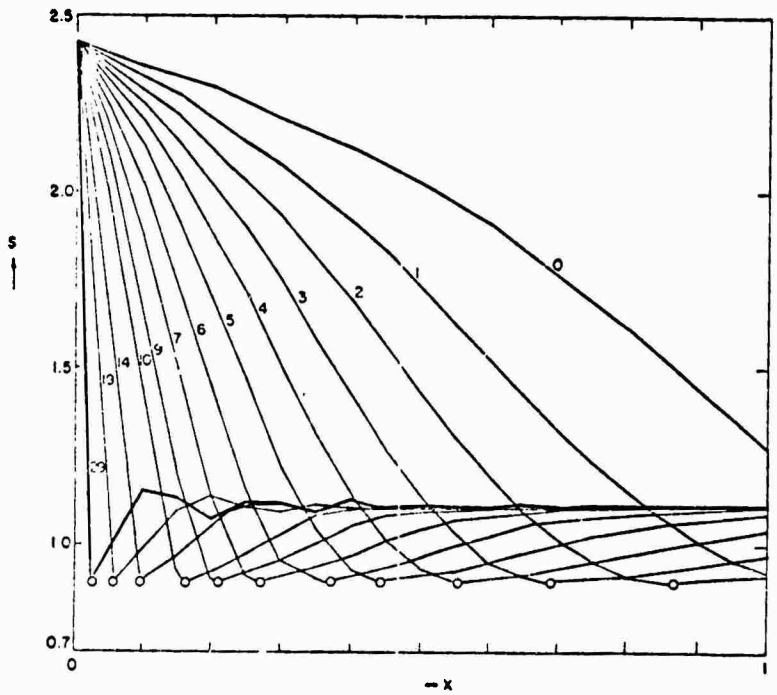

Fig. 13. Entropy Distribution Across Shock Layer at Different Distances from the Nose; Explicit Fit of the Point of Minimum Entropy; n=20

of 10 initial intervals. The improvement is now complete.

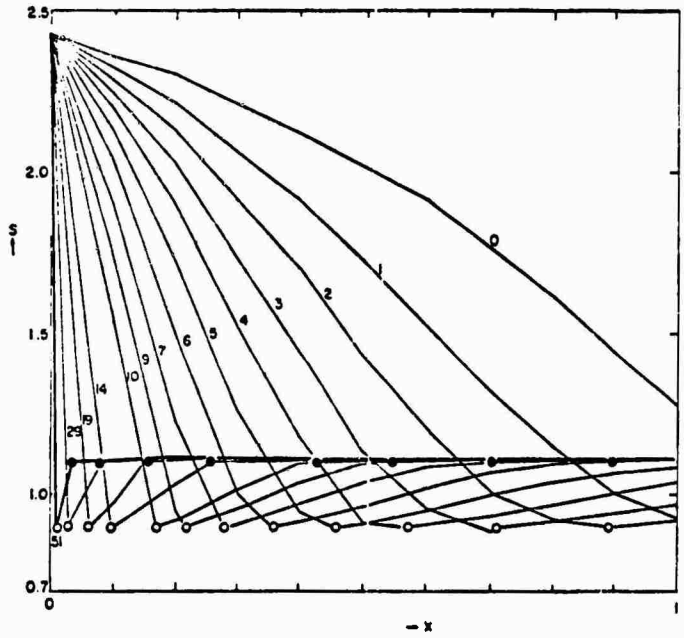

Fig. 14 Entropy Distribution Across Shock Layer at Different Distances From the Nose; Explicit Fit of Two Lines of Constant Entropy; n=10.

It is clear that, by using the device of tracking two streamlines, the entire shock layer can be computed to any distance from the body nose with only 10 intervals across, with a very simple code (equally spaced nodes), provided that shock and body points are carefully treated as explained in Section III.

It may be added that the stations at which the computed entropy layer thickness becomes 0.1 or 0.05 of the shock layer thickness agree very well with the predictions shown in Figs. 3 and 4.

IX. REFERENCES

1. Hayes, W.D. and Probstein, R.F.: Hypersonic Flow Theory, Vol. I, Second Edition, Academic Press, 1966.
2. Moretti, G.: Inviscid Blunt Body Shock Layers, Two-Dimensional Symmetric and Axisymmetric Flows, Polytechnic Institute of Brooklyn, PIBAL Report No. 68-15, June 1968.
3. Courant, R., Friedrichs, K.O. and Lewy, H.: Ueber die partiellen Differenzgleichungen der mathematischen Physik, Math. Ann. 100, 32, 1928.
4. Moretti, G.: The Choice of a Time-Dependent Technique in Gas Dynamics, Polytechnic Institute of Brooklyn, PIBAL Report No. 69-26, July 1969.
5. Moretti, G. and Abbett, M: A Time-Dependent Computational Method for Blunt Body Flows, AIAA Journal, 4, 2136, 1966.
6. Kentzer, C.P.: Discretization of Boundary Conditions on Moving Discontinuities, Proc. 2nd Internation Conference on Numerical Methods in Fluid Dynamics, M. Holt, ed., Springer-Verlag, (Lecture Notes in Physics, 8), pp. 108, 1971.
7. Moretti, G.: Thoughts and Afterthoughts About Shock Computations, to be published as a PIBAL Report.
8. Abbett, M.: Boundary Conditions for Computational Procedures for Inviscid Supersonic Steady Flow Field Calculations, Aerotherm Rept. 71-41, 1971.
9. Moretti, G.: Importance of Boundary Conditions in the Numerical Treatment of Hyperbolic Equations, Phys. Fluids, Supplement II, 12, 12, Part II, pp. II-13, 1969.
10. Moretti, G.: Complicated One-Dimensional Flows, Polytechnic Institute of Brooklyn, PIBAL Report No. 71-25, September 1971.